Transient Structures and Kinetics of the Ferrioxalate Redox Reaction Studied by Time-Resolved EXAFS, Optical Spectroscopy, and DFT[†]

Jie Chen,[‡] Hua Zhang,[‡] Ivan V. Tomov,[‡] Max Wolfsberg,[‡] Xunliang Ding,[§] and Peter M. Rentzepis*,[‡]

Department of Chemistry, University of California, Irvine, California 92697 and Institute of Low Energy Nuclear Physics, Beijing Normal University, Beijing 100875, China

Received: May 1, 2007

The photoredox reaction transients of ferrioxalate in water have been studied by means of time-resolved EXAFS and ultrafast optical transient spectroscopy. The transient spectra and kinetics have been measured from the femtosecond to millisecond range, and the Fe−O bond lengths of the ferrioxalate redox reaction transients have been determined with 2 ps time resolution and 0.04 Å accuracy. These data in conjunction with quantum-chemistry DFT and UHF calculations were used to formulate a mechanism for the Fe(III) to Fe(II) redox reaction where dissociation precedes electron transfer. In addition, radical scavenging experiments support the mechanism proposed.
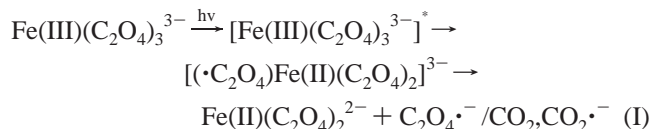
1. Introduction

1.1. Photochemistry of Ferrioxalate. Since Draper suggested that the Fe(III) to Fe(II) redox reaction may find applications in photometry,[1] the redox reaction of ferrioxalate solution has been studied widely.[2−7] The ferrioxalate redox reaction has also been used as a precise actinometer,[8] and its photochemistry has been studied by several techniques including flash photolysis and electroanalysis.[5,7,9,10] It is generally accepted[4−7] that light induces electron transfer that reduces the $Fe(III)(C_2O_4)_3^{3-}$ complex to the Fe(II) complex with the overall photoreaction written as:[5]

$$2Fe(C_2O_4)_3^{3-} + h\nu \rightarrow 2Fe(C_2O_4)_2^{2-} + C_2O_4^{2-} + 2CO_2\uparrow$$

Two distinctly different proposals for the primary reaction after excitation have been proposed:[4−7]
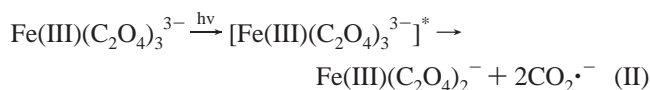
(I) Intramolecular electron transfer: in this mechanism, electron transfer from the oxalate to Fe(III) takes place immediately after photoexcitation. This mechanism was first proposed in 1954[11] and expanded in 1959[4] by Parker et al. when long-lived intermediates were observed by flash photolysis, eq I.

$$Fe(III)(C_2O_4)_3^{3-} \xrightarrow{h\nu} [Fe(III)(C_2O_4)_3^{3-}]^* \rightarrow$$
$$[(\cdot C_2O_4)Fe(II)(C_2O_4)_2]^{3-} \rightarrow$$
$$Fe(II)(C_2O_4)_2^{2-} + C_2O_4{}^{\bullet -}/CO_2,CO_2{}^{\bullet -} \quad (I)$$

The $[(\cdot C_2O_4)Fe(II)(C_2O_4)_2]^{3-}$ complex was suggested to be metastable and formed after one electron was transferred from the oxalate to Fe(III). This complex consisted of both Fe(II) and $C_2O_4{}^{\bullet -}$ radical. The $C_2O_4{}^{\bullet -}$ or $CO_2{}^{\bullet -}$ radicals were formed according to this mechanism after the cleavage of one oxalate ligand.

(II) Dissociation of ferrioxalate: according to this mechanism, shown in eq II, intramolecular electron transfer is not the primary process, but it follows the cleavage of an Fe(III)−O bond, between one oxalate ligand and the iron, and the breakage of the C−C bond before electron transfer.

$$Fe(III)(C_2O_4)_3^{3-} \xrightarrow{h\nu} [Fe(III)(C_2O_4)_3^{3-}]^* \rightarrow$$
$$Fe(III)(C_2O_4)_2^{-} + 2CO_2{}^{\bullet -} \quad (II)$$

Cooper et al. performed microsecond experiments in 1971[5] and, based on the transient spectra observed, concluded that the primary redox reaction may involve electron transfer, dissociation, or both. However, these authors could not distinguish between the two mechanisms because of the low time resolution of their experiments. The $Fe(III)(C_2O_4)_2^{-}$ transient suggested by mechanism II[5] has been detected experimentally by us recently using femtosecond optical and EXAFS spectroscopy and supported by DFT and UHF quantum-chemistry calculations.[7] This transient is formed within 5 ps and has a decay lifetime in the nanosecond range. The sequence of the cleavage of Fe(III)−O bond and the C−C bond could not be resolved because only Fe−O bond distances were observed and measured by our EXAFS experiments. However, some electroanalytical flash photolysis measurements of the ferrioxalate redox reaction have shown that the Fe(III) complex remains in the Fe(III) oxidation state, initially, after the "flash", and it was suggested that the initial intermediate is a ferric diradical, which is the result of C−C bond cleavage.[12] [13]C isotope effects were observed in the 366−520 nm range;[10] this observation suggested that the C−C bond cleavage may be the rate-controlling step.

In both mechanisms I and II, the $C_2O_4{}^{\bullet -}$ or $CO_2{}^{\bullet -}$ anion radicals are expected to be formed. These radicals are known to react further with $Fe(III)(C_2O_4)_3^{3-}$ molecules to yield an additional Fe(II) product that leads to an overall quantum yield for the Fe(III) to Fe(II) redox reaction larger than 1. The formation of $C_2O_4{}^{\bullet -}$ or $CO_2{}^{\bullet -}$ radicals was confirmed by electron paramagnetic resonance[13] and the initiation of photopolymerization of vinyl monomers.[14] Distinguishing between the $C_2O_4{}^{\bullet -}$ and $CO_2{}^{\bullet -}$ radicals has not been reported until now; however, it has been suggested that the radical observed is $CO_2{}^{\bullet -}$ because $C_2O_4{}^{\bullet -}$ was reported to undergo decarboxylation at a rate of at least 2×10^6 s^{-1}.[15]

EXAFS Transient Structures and Kinetics of Fe(III)ox

J. Phys. Chem. A, Vol. 111, No. 38, 2007 **9327**

In summary, the major uncertainty in the photoredox reaction mechanism of ferrioxalate lies on our understanding of the nature of this process. Is it true that when the ferrioxalate molecule is excited within what is called the charge-transfer (CT) band intramolecular electron transfer automatically takes place? Or is time required for the excited molecule to reorient in order to match the proper configuration for intramolecular electron transfer? If it does, how fast is the reorientation? Is it possible that dissociation takes place during the time required to achieve a suitable orientation for electron transfer? We shall try to answer some of these questions.

1.2. Ultrafast Extended X-ray Absorption Fine Structure (EXAFS). The development of ultrafast, powerful lasers has made it possible to perform time-resolved studies not only in optical spectroscopy but also in other areas such as X-ray and electron-beam spectroscopy. We have used a femtosecond laser-driven plasma to generate intense ultrashort X-ray pulses[16−18] of characteristic lines and continua, in the keV range, with subpicosecond duration, through the interaction of high-power femtosecond laser pulses with solid and liquid targets.[19] Such pulsed X-ray systems have been utilized for X-ray diffraction and X-ray absorption studies that include transient structures with subangstrom spatial and picosecond time resolution.[7,20] The pump/probe technique[21] used in ultrafast optical time-resolved measurements has also been applied to hard X-ray diffraction and absorption studies.[22] In this case, the ultrashort X-ray pulses are used to probe the structure changes as a function of time after excitation and, therefore, they are precisely synchronized with the exciting optical pulses. Accurate synchronization can be achieved because both the X-ray and optical pulses are generated from the same laser source. X-ray diffraction, which is the most-useful method for the study of structure of solids on the atomic level, finds limited application in the liquid phase. It is, however, supplemented by X-ray absorption spectroscopy (XAS), which has been shown to yield the structure of molecules in the liquid phase.[23] For example, X-ray absorption near-edge structure (XANES) spectroscopy measures the electronic structure, charge distribution, and oxidation−reduction of the atom. In addition, valuable structural information including chemical bonding of molecules and coordination numbers may be determined by the use of extended X-ray absorption fine structure (EXAFS) spectroscopy.

In recent years, ultrafast pump/probe X-ray studies of liquid samples have been used to reveal the structure of molecular transients in solution formed after excitation with ultrafast optical pulses.[24,25] The advances in time-resolved XAS have been reviewed recently;[26,27] however, so far very few time-resolved ultrafast X-ray absorption studies have been reported, and most of these are concerned with the study of the structure of transient species of coordination compounds such as [Ru(bpy)$_3$]$^{2+}$. The oxidation state change of the central Ru atom after excitation has also been observed with a temporal resolution of 100 ps by excited-state XANES[28] and found to be in agreement with the simulation of the transient XANES spectrum;[29] a Ru−N bond contraction by ∼0.03 Å in the excited-state complex 50 ps after excitation has also been measured by ultrafast EXAFS.[30] Recent time-resolved XAS studies have been focused on iron[31,32] and copper[33,34] complexes. Photoexcited Fe(CN)$_6^{4-}$ in water has been studied using a laser-based tabletop X-ray system, which utilizes a polycapillary X-ray lens to increase the X-ray flux at the sample. XAS spectra at −40, 0, and +30 ps were recorded with 30 ps resolution.[32]

In this paper, we present experimental EXAFS data obtained from a tabletop laser system that generates femtosecond hard X-ray pulses in the 5−25 KeV range. In this experiment, we use 6.5−8.5 keV X-rays because they include the Fe K-edge and ∼1000 eV higher energy required by the EXAFS experiments. The time-resolved X-ray absorption studies presented in this paper were aimed to measure the changes in the structure induced by a 400 nm femtosecond laser pulse that initiates the Fe(III) → Fe(II) redox reaction of ferrioxalate in water. In a previous short communication,[7] we have reported the structure of transients formed during the first few picoseconds after excitation. In this article, we present and discuss time-resolved optical data obtained from $t = 0$ to milliseconds after excitation. In addition, EXAFS and quantum-chemistry DFT and UHF calculations relating to the structure of intermediates are presented. Radical scavenging experiments were performed in order to help us distinguish between mechanisms I and II. On the basis of these data, an extended mechanism of ferrioxalate photochemistry will be proposed and discussed in some detail in the following sections of this paper.

2. Experimental Details

2.1. Time-Resolved Optical Measurements. The optical systems for time-resolved spectroscopic experiments have been described and used for the photolysis of CBr$_4$ previously,[35] which consist of three laser systems that were used to obtain femtosecond (fs) to millisecond (ms) transient absorption spectra. A typical ultrafast pump/probe absorption laser system composed of a Ti:Sapphire laser emitting 130 fs pulses at 800 nm was used for the optical fs to picosecond (ps) experiments. The transient spectra were detected and analyzed by an air-cooling charge-coupled device, CCD. The pump pulse for the fs experiments was the 400 nm second harmonic of Ti: Sapphire laser. The optical probe beam consisted of a broad continuum that covered the 400−800 nm region and was of the same time duration, 100 fs, as the pump pulse, The ps to nanosecond (ns) transient experiments were performed using a Nd:YAG laser that emitted 25 ps pulses. In addition, a 6 ns Nd:YAG laser was employed for the ns to ms experiments. The 355 nm third harmonic of the fundamental pulse was used in both ps and ns experiments as the pump pulse. The 360−700 nm continuum probe beam used for the ps/ns experiments was produced by focusing the 1064 nm fundamental beam into a 15 cm water cell. Dispersion broadening added 9 ps to the probe pulse. The 360−850 nm continua for the ns/ms experiments were generated by a flash lamp. The detectors used were either a CCD coupled to a computer for the fs/ps and ps/ns experiments or a fast photomultiplier (Hamamatsu R928) coupled to an oscilloscope for ns lived transient spectra.

2.2. Time-Resolved EXAFS Experiments. (NH$_4$)$_3$Fe(III)-(ox)$_3$·nH$_2$O, where ox = C$_2$O$_4^{2-}$, was purchased from Alfa Aesar and dissolved in distilled water. A homemade 2-mm-wide stainless steel nozzle formed a 100-μm-thick liquid jet. The ferrioxalate solution was poured through the jet and circulated through a 100 mL reservoir. Pulses (100 fs, 0.5 mJ, 400 nm) were focused by a cylindrical lens on the sample with an intensity of 3 × 10^{12} W/cm^2, which is sufficient energy to excite and photodissociate the sample (400 nm = 3.1 eV, calculated Fe−O bond energy = 0.66 eV). The concentration of Fe(III) oxalate used for the time-resolved EXAFS experiments were 1.6 mol/L in water. This concentration corresponds to μx ≈ 1 (μ is the X-ray mass absorption coefficient, and x is the length of the X-ray's path through the sample) for 7.1 keV radiation and an OD ≈ 3.5 (OD = absorbance) at the 400 nm wavelength of the pump pulse. Therefore, in the 10^{-9} mL excitation volume, each 400 nm pump pulse excited only 20%
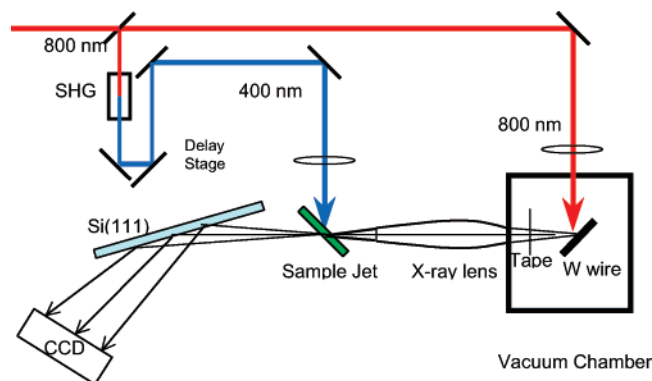
9328 *J. Phys. Chem. A, Vol. 111, No. 38, 2007*

Chen et al.

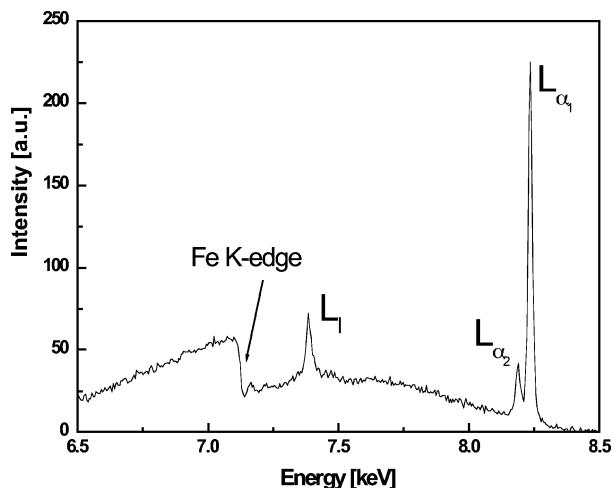**Figure 1.** Dispersive ultrafast X-ray absorption spectrometer.

Figure 2. X-ray continuum spectra in the vicinity of the iron K edge.

of the ferrioxalate molecules. As a result, the amount of Fe(II) product formed was negligible compared to the 100 mL total volume. Therefore, repeated multiple shot experiments performed with a 100 mL sample did not affect the accuracy of the data; however, the sample was frequently discarded and replenished with fresh solution. The 0.6 ps duration X-ray pulses were generated by a tabletop ultrashort X-ray source system, which has been reported previously by us in conjunction with time-resolved X-ray diffraction experiments.[17,20] The ultrafast X-ray absorption system has also been reported previously;[7] therefore, only a schematic representation is shown in Figure 1. There are three major differences between time-resolved EXAFS and X-ray diffraction.

(1) Continuum generation: Tungsten wire was selected as the target because it generates intense X-ray continuum owing to its high *Z* number. A 0.25-mm-diameter tungsten wire was found to generate intense X-ray continuum and not rupture by the intense laser pulses. The 0.6 ps upper limit of the X-ray pulse duration was determined by the thin crystal technique.[17] We were able to record simultaneously the entire ~1000 eV XAS spectrum using a dispersive X-ray spectrometer,[36] see Figure 1. Therefore, we did not have to perform point-by-point measurements and consequently avoid the inaccuracy caused by the pulse-to-pulse laser and X-ray intensity fluctuations. The continuum spectrum in the vicinity of the Fe K edge, 7.1 keV, identified by an arrow is shown in Figure 2. Several tungsten lines, $L_{\alpha1}$, $L_{\alpha2}$, and L_l, were also detected in the same region, which were used for accurate energy calibration of the EXAFS spectrum. In this configuration, the resolution provided by the system was estimated to be 20 eV, which is consistent with the

observed 22 eV line width of the $L_{\alpha1}$ line (the actual line width is 6.6 eV).

(2) X-ray flux: The X-ray flux, in the 7−8 keV energy range, was estimated to be 1.9×10^7 photon/(s·4π) after correction for absorption along the X-ray's path as well as the detector efficiency, assuming that the X-ray emission is isotropic in 4π steradians. It was determined that the X-ray lens, which is used to focus the X-rays on the sample, increased the X-ray flux on the sample more than 100-fold. To further optimize the X-ray flux, we positioned the X-ray lens such that the short focal length faced the source.[17] This was important because of the smaller focus spot size produced by the short focal length, which is ~80 μm at 7−8 keV. This size is very close to the size of the X-ray source at the wire and therefore increased the input solid angle and the number of collected X-ray photons. In addition, the output divergence was reduced to 3°, which is still larger than the minimum 2.2° divergence required by the dispersive spectrometer.

(3) Uniform excitation: A uniformly excited and probed sample is very important for EXAFS experiments. However, the penetration length of UV light is too short compared to that of the probing X-rays. When the 400 nm pulses were focused tightly, breakdown in the sample solution occurred (bubbles appeared). We achieved homogeneous excitation of the ferrioxalate molecules by adjusting the path of the probe X-ray beam to be perpendicular to the path of the UV beam, and both intersecting the jet flow at 45° angles, see Figure 1. This arrangement of the beams allowed for the pump pulses to excite the maximum amount of sample molecules and also allowed the X-ray pulses to probe the largest possible fraction of the excited molecules. Spatial overlap of the optical pump and X-ray probe beams was achieved by transmitting both beams through a 100 μm tungsten pinhole placed at the position of the sample jet. The time synchronization of the optical pump and X-ray probe pulses was also accurately established to within 1 ps by the nonlinear method described previously.[20] The time of maximum overlap of optical and X-ray pulses defined the zero excitation time for the time-resolved EXAFS experiments. Other times before and after excitation were obtained by the appropriate delay of the pump pulses.

2.3. EXAFS Data Analysis The structures of the intermediates evolved during the course of the $Fe(III)(C_2O_4)_3^{3-}$ redox photochemical reaction was determined by analysis of the EXAFS spectra recorded between −20 ps and +115 ps after excitation. The EXAFS spectra of the ferrioxalate molecule obtained in the form of μx versus X-ray energy, *E*, at −20 ps before excitation and +25 ps after excitation are shown in Figure 3. A standard automated data-reduction procedure (ATHENA program[37]) was used to analyze the EXAFS raw data. The EXAFS spectrum of the X-rays passing through air was used as the background spectrum for subtraction.

The crystal structure of $(NH_4)_3Fe(III)(C_2O_4)_3\cdot3H_2O^{38}$ published previously formed the basis for the simulation of the $Fe(III)(C_2O_4)_3^{3-}$ EXAFS spectra by means of the FEFF 8.20 code.[39] The influence of the cation NH_4^+ and solvent on the structure were not considered in our calculations. The first shell Fe−O path was utilized to perform the necessary phase-shift correction, and the μx versus *E* spectra were then transformed to $|\chi(R)|$ versus *R* spectra. Figure 4 displays the bond length for the first two coordination shells, the absorbing iron, and neighboring atoms. This discussion will be limited to the first coordination shell, which corresponds to the Fe−O bond length.

2.4. Theoretical Calculations of Fe−O Bond Length. These calculations were restricted to the first coordination shell of the

EXAFS Transient Structures and Kinetics of Fe(III)ox

J. Phys. Chem. A, Vol. 111, No. 38, 2007 **9329**
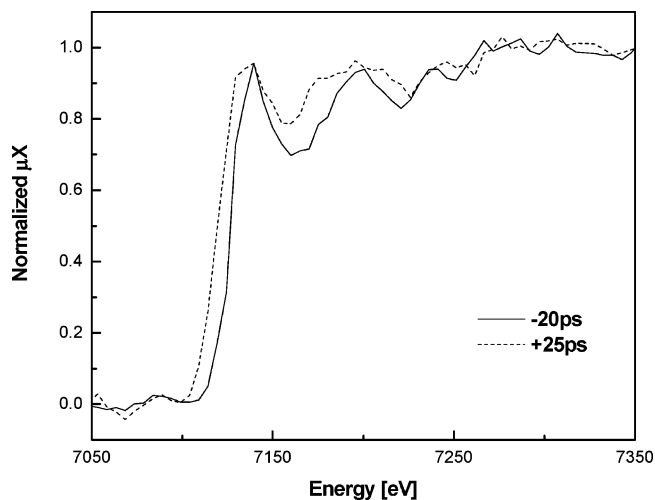
Figure 3. EXAFS spectra recorded at -20 ps (before excitation, solid) and $+25$ ps (after excitation, dot).
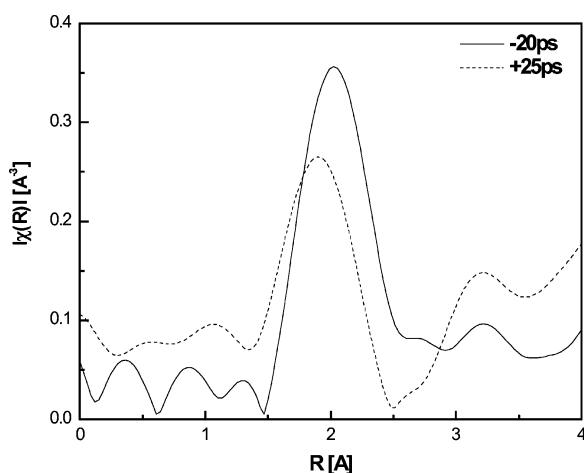
Figure 4. *R*-space EXAFS spectra of ferrioxalate/water solution before (solid, -20ps) and after (point, $+25$ps) UV radiation.

Fe ionic species. This means that iron oxalate complexes were the subjects of the calculations without consideration of solvation effects. Also, no spin orbital coupling was considered (a usual assumption is such calculations). Geometry optimizations were carried out with the Gaussian 03 program.[40] These were carried out at the UHF/6-31G and B3LYP/6-31G levels. All of the reported calculations were carried out with the high-spin states $S = ^5/_2$ and $S = 2$ for Fe(III) and Fe(II) complexes, respectively. In some (though not all) cases, we explicitly showed that the high-spin complexes are indeed the low-energy states, as expected. The results for the calculated Fe$-$O bond distances along with the geometries are reported in Table 1 along with the EXAFS findings. The optimizations have been tested in most cases to correspond to true minima by calculations showing that there are $3N - 6$ real vibrational frequencies. The Fe(III)(C$_2$O$_4$)$_3^{3-}$ ion was found to have symmetry D_3, whereas the symmetries of Fe(III)(C$_2$O$_4$)$_2^{2-}$ and Fe(II)(C$_2$O$_4$)$_2^{-2}$ were both found to be D_{2d}. The TURBOMOLE program has capabilities to calculate the geometries and energies of excited electronic states by the TDDFT method. It is our intention to use this method to explore the systems under consideration further.

2.5. Radical Scavenging Experiments. The sample consisted of a 5.8×10^{-5} M solution of ferrioxalate in water to which $0-5.0 \times 10^{-3}$ M of thymine, an anion radical scavenger was added. The solution was placed in a 10 cm optical path length cell and irradiated for intervals of time varying from 10 to 400

TABLE 1: Fe$-$O Bond Length at Various Delay Times before and after Excitation Obtained by Time-Resolved EXAFS and Quantum-Chemistry Calculations Using the Gaussian 03 Program

delay time	assignment	ligand	exptl R(Å)	calcd R(Å) UHF	DFT
-20 ps	Fe(III)(C$_2$O$_4$)$_3^{3-}$	C$_2$O$_4$	2.02	2.04	2.01
$1-2$ ps	[Fe(C$_2$O$_4$)$_3^{3-}$][a]	C$_2$O$_4$	2.16	N/A	N/A
4 ps	[C$_2$O$_3$O$-$Fe(III)(C$_2$O$_4$)$_2$]$^{3-}$	C$_2$O$_3$O	1.93$-$2.09	1.87	1.87
		C$_2$O$_4$		2.01	2.02
$9-115$ ps	Fe(III)(C$_2$O$_4$)$_2^-$ tetrahedral-like	C$_2$O$_4$	1.87$-$1.93	1.90	1.90
110 ns$-$2 ms	Fe(II)(C$_2$O$_4$)$_3^{4-}$	C$_2$O$_4$	N/A	N/A	N/A
	Fe(II)(C$_2$O$_4$)$_2^{2-}$ tetrahedral-like			2.04	2.01
final product	[Fe(II)(C$_2$O$_4$)$_2$(H$_2$O)$_2$]$^{2-}$	H$_2$O	2.11[a]	2.15	N/A
		C$_2$O$_4$	2.20[a]	2.16	N/A

[a] Reference 44.
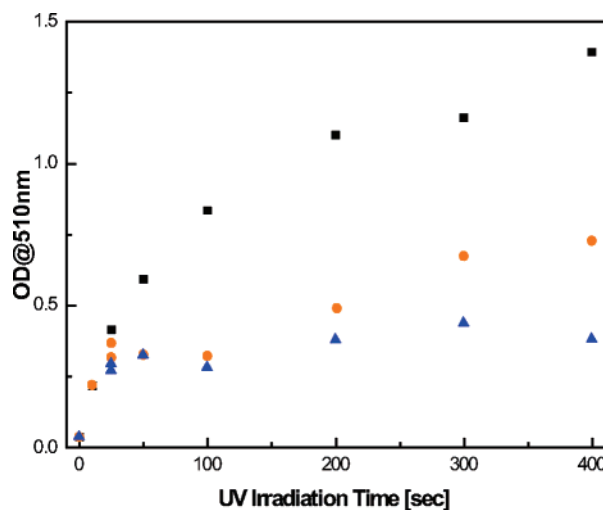
Figure 5. Optical density of [Fe(II)(phen)$_3$]$^{2+}$ complex at 510 nm plotted as a function of irradiation time.

s, while being stirred constantly. The excitation wavelength range of $300-500$ nm was provided by a 150 W ORIEL high-pressure xenon lamp and BG-25 filter to determine the efficiency of the thymine as a CO$_2^{\bullet-}$ scavenger; the concentration of thymine varied from 0 to 5.0×10^{-3} M. Because the amount of the Fe(II) photoredox product depends on the amount of CO$_2^{\bullet-}$ available to react with the Fe(III) complex to produce the Fe(II) product, it was measured immediately after photolysis by the addition of 1,10-phenanthroline (phen) following the procedure described in the literature.[41] The optical density at the maximum absorption of the [Fe(II)(phen)$_3$]$^{2+}$ complex (λ_{max} = 510 nm) was measured and plotted as a function of irradiation time in Figure 5.

3. Results and Discussion

The experimental data for the photoredox of ferrioxalate dissolved in water presented in this paper were obtained in air at room temperature. The effect of oxygen can be neglected when the concentration of ferrioxalate is higher than 1 mM.[42] The absorption spectrum of Fe(III)(C$_2$O$_4$)$_3^{3-}$ in water, shown in Figure 6, consists of two broad bands with maxima at 210 nm ($\epsilon = 1.2 \times 10^4$ cm^{-1}M^{-1}) and at 669 nm ($\epsilon = 0.94$ cm^{-1}M^{-1}).

3.1. Kinetics of Ferrioxalate Photoredox Reaction. Our fs/ps optical data show that after excitation at 400 nm ($\epsilon =160$ cm^{-1}M^{-1}) a fast transient absorption band is formed, whose maximum wavelength red shifts continuously until it reaches

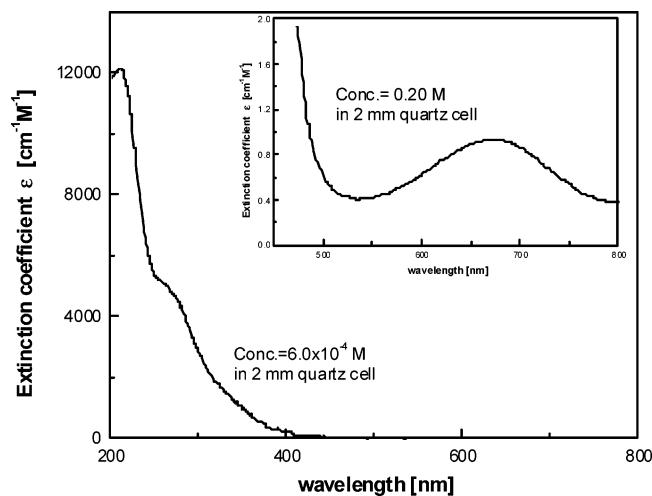**9330** *J. Phys. Chem. A, Vol. 111, No. 38, 2007*

Chen et al.

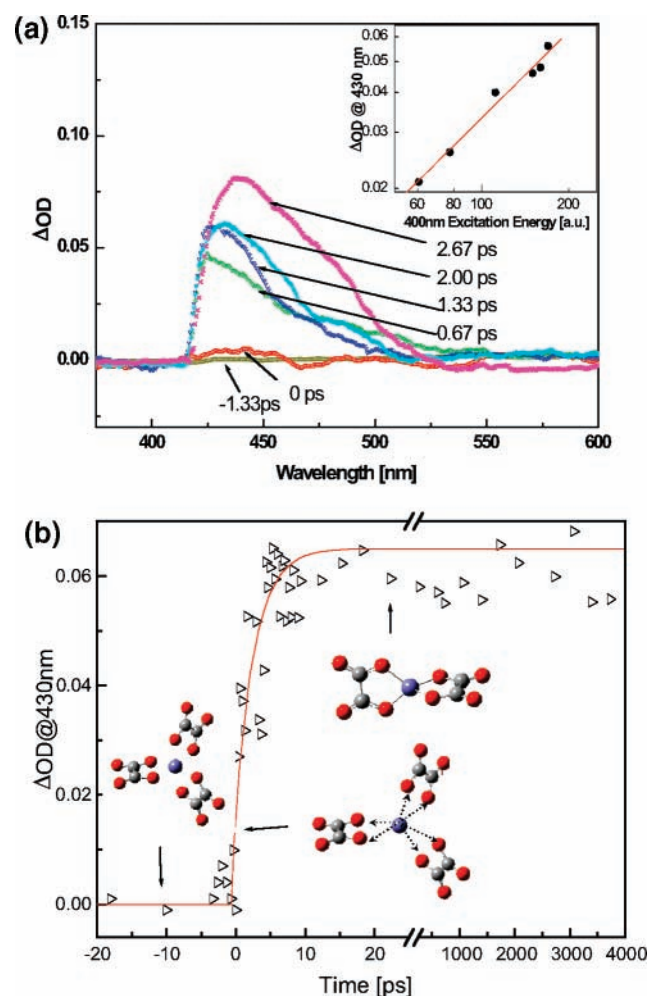**Figure 6.** Absorption spectrum of ferrioxalate/water solution.

Figure 7. (a) Picosecond transient absorption spectra of ferrioxalate in water. (b) Formation kinetics: -20 to 25 ps ($C = 0.115$ M, excitation at 400 nm) and 250 ps to 4 ns ($C = 9.3 \times 10^{-3}$ M, excitation at 355 nm). The three structures illustrated represent the ground state (-20 ps to -1 ps), the excited state (0 ps to $+2$ ps), and the tetrahedral-like Fe(III)(C$_2$O$_4$)$_2^-$ transient(10 ps to 4 ns).

430 nm. The shift in the spectra from -1.33 to 2.67 ps is shown in Figure 7a. A similar transient absorption band and linear dependence was also observed in the ps/ns experiments with 355 nm excitation. This transient spectrum achieves its maximum intensity 2.6 ps after excitation then remains constant for
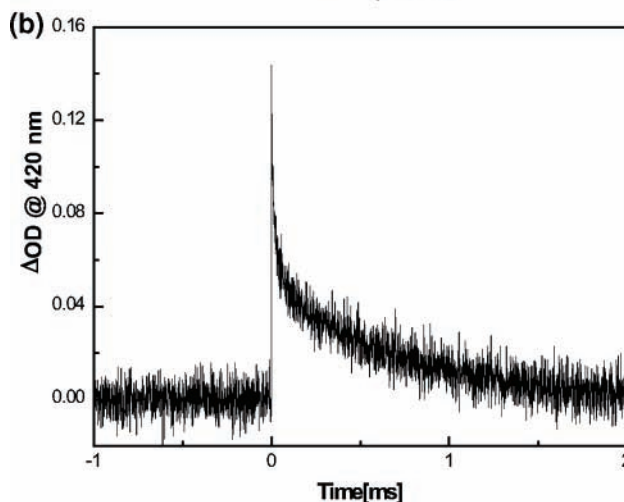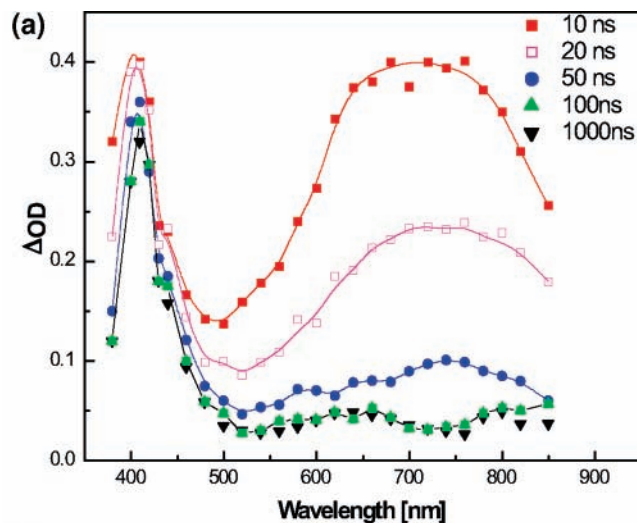

Figure 8. Nanosecond transient absorption spectra and kinetics of 2.3 $\times$ 10^{-3} M ferrioxalate in water, irradiated with 355 nm pulses.

at least 4 ns as depicted in Figure 7b. The inset in Figure 7a shows that the absorbance of this transient depends linearly on excitation intensity; therefore, we are monitoring a one-photon process. Another transient with similar absorption bands shown in Figure 8a is formed immediately after ns/ms pulse excitation in experiments. Both 400 and 355 nm excitation levels are located at the tail end of the 210 nm ferrioxalate, absorption band, shown in Figure 6. Therefore, we assign the transient absorption bands observed in the 2.6 ps$-$10 ns range to the same transient, which is formed within 2.6 ps and does not decay for at least 10 ns. We also observed that, when much higher pulse intensities were used for excitation, a new transient band was detected in the 500$-$650 nm range formed primarily by a two-photon process. Two similar transient bands between 360$-$550 nm and 500$-$850 nm were also observed in the ns range, also corresponding to one- and two- photon processes respectively, see Figure 8a. We shall discuss only the 400 nm or 355 nm one-photon processes because this band is relevant to the one-photon redox processes that we are concerned with. The absorption bands detected by the ns/ms experiments that are shown in Figure 8a were also observed by Nadtochenko and Kiwi 100 ns after excitation.[6] This 360$-$550 nm nanosecond transient absorption band observed was found to have a two-component decay. The decay kinetics at 420 nm at a concentration of 2.3 mM is shown in Figure 8b. The fast and long-lived components have a decay lifetime of 110 ns and 0.63 ms at 2.3

EXAFS Transient Structures and Kinetics of Fe(III)ox

J. Phys. Chem. A, Vol. 111, No. 38, 2007 **9331**

mM, respectively. Both decays were found to be diffusion-controlled and depend upon the concentration of ferrioxalate.

3.2. Histogram of Fe−O Bond Length Change. The ultrafast EXAFS data presented here and in ref 7 provide new information not known before concerning the Fe−O bond length of the intermediate species formed during the photoredox reaction. These ultrafast EXAFS data indicate that the Fe−O bond length has a value of 2.00 Å in the original nonirradiated molecule, which increases to 2.16 Å during the first 2 ps after excitation followed by a Fe−O value of 1.93 Å after 4 ps that becomes 1.87 Å after 9 ps. The time-resolved EXAFS and optical data have been compared with quantum-chemistry DFT and UHF calculations. After analyzing the experimental and theoretical calculation data, we propose a mechanism for the redox Fe(III)/Fe(II) reaction that includes a sequence of the dissociation and electron-transfer processes.

(a) Before excitation. The reliability of the EXAFS data was determined by comparing the value of the Fe−O bond of the stable parent $Fe(III)(C_2O_4)_3^{3-}$ ion complex obtained by our time-resolved EXAFS system with the value in the literature.[38] $Fe(III)(C_2O_4)_3^{3-}$ is a highly symmetric ion for which DFT calculations predict a value for the Fe(III)−O bond distance of 2.01 Å, which is found to be close to the experimental values of 2.00 Å in crystal[38] and the calculated value of 1.979−2.024 Å in ref 43. The agreement of bond length values confirm that $Fe(III)(C_2O_4)_3^{3-}$ is a good model for the calculation of the Fe−O bond length for both solution and crystal samples. Using our time-resolved EXAFS experimental system, we determined that the Fe(III)−O distance of the parent molecule 20 ps before excitation is 2.02 Å, which is in good agreement with the literature value of Fe(III)−O for crystalline $Fe(III)(C_2O_4)_3^{3-}$ and the DFT calculated Fe−O distance. In addition, we performed CW EXAFS experiments using the same sample, without excitation, and determined the Fe(III)−O bond length to be 1.98 Å. In summary, because our experimental Fe−O values agree quite well with the experimental and theoretical literature values, we believe that the data obtained by our ultrafast EXAFS system are reliable within 0.04 Å accuracy. We can also conclude that the −20 ps EXAFS spectrum of the parent molecule is correctly assigned to the $Fe(III)(C_2O_4)_3^{3-}$ by performing back Fourier transformation between the wave vector spectra in *q* space obtained with the CW X-ray instrument and at −20 ps obtained with the fs X-ray system.

(b) Zero to two ps after excitation (reaction 1).

$$Fe(III)(C_2O_4)_3^{3-} \xrightarrow{\text{hv}} [Fe(C_2O_4)_3^{3-}]^* \qquad (1)$$
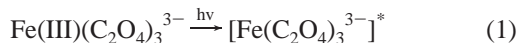
Previous ns to ms studies[5,6] have proposed the formation of an electron-transfer excited state $Fe(II)(C_2O_4)_3^{3-}$ to be the first intermediate of the photoredox reaction. However, our data suggest that the oxalate to Fe(III) electron-transfer process is not the initial process, but the molecule retains its +3 valence in the excited state. During the first 2 ps, an intermediate state is observed by our ultrafast optical experiments and time-resolved EXAFS, which, as already noted, has a Fe−O distance of 2.16 Å. Within these first 2 ps after excitation, the original 2.02 Å Fe(III)−O distance has been elongated by about 0.2 Å. This transient was assigned to an excited state of the parent Fe(III) molecule. On the basis of the Fe−O bond distance of the intermediates formed after 4 ps, this transient retains the Fe(III) charge, and therefore we assign this excited state to be $[Fe(C_2O_4)_3^{3-}]^*$ without any electron transfer or ligand dissociation having occurred at this time. However, we must note that the configuration of the excited state is strained and the bond

elongation weakens the covalent bond between iron and oxygen. Although electron transfer from oxalate to the iron does not take place at this time, the electron density of the excited LUMO orbital of Fe(III) has increased compared to the ground state, which could be understood as a partial charge transfer.[7]

(c) Two to six hundred and ten ps after excitation (reaction 2).

$$[Fe(C_2O_4)_3^{3-}]^* \rightarrow (C_2O_3)O - Fe(III)(C_2O_4)_2^{3-} \rightarrow$$
$$Fe(III)(C_2O_4)_2^- + 2CO_2\cdot^- \quad (2)$$
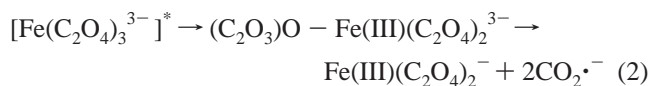
Time-resolved EXAFS experiments between 4 and 115 ps after excitation reveal that the Fe−O bond length varies between 1.87 and 1.93 Å. These Fe−O values are shorter by 0.09−0.15 Å than that of the stable parent molecule of 2.02 Å and much shorter than the known Fe(II)−O bond distance of 2.11−2.22 Å. In addition, we performed DFT and UHF calculations to help us interpret these results and assign the EXAFS measured Fe−O bond distances to transient iron oxalate species.

First, Fe(II)(ox) complexes were eliminated as possible intermediates because of the large discrepancy between the Fe(II)−O and the observed Fe−O bond distances of the transients form during the 2−115 ps. $Fe(II)(C_2O_4)_2^{2-}$ is predicted by DFT and UHF to have a tetrahedral-like structure, which has D_{2d} symmetry, and the dihedral angle between two oxalate planes is close to 90°. The $Fe(II)(C_2O_4)_2^{2-}$ Fe−O distance was calculated by UHF and DFT to be 2.04 and 2.01 Å, respectively. We note that the four-coordinate complexes are thought to be more-flexible than the original six-coordinate complexes. In addition, $Fe(II)(C_2O_4)_3^{3-}$ or $Fe(II)(C_2O_4)_3^{4-}$ have one more oxalate ligand; therefore, their Fe(II)−O bond length is expected to be even longer than that of $Fe(II)(C_2O_4)_2^{2-}$ and much larger than the 1.87−1.93 Å bond length observed.

Second, the formation of $Fe(ox)(H_2O)$ complexes involves the combination of Fe(ox) and H2O, which are diffusion-controlled reactions and therefore should take place in the ns range or longer. The final redox product is hydrated Fe(II)(ox), $Fe(II)C_2O_4\cdot2H_2O$ with measured Fe(II)−O bond lengths of 2.22 Å for Fe(II)−ox and 2.11 Å for Fe(II)−OH2.[44] Therefore, it seems improbable that $Fe(ox)(H_2O)$ is an intermediate formed in the ps range.

Third, the structures of several Fe(III)(ox) complexes calculated by UHF and DFT quantum chemistry is listed in Table 1. However, to our knowledge no experimental data concerning the structures of these Fe(III) transients have been reported. $Fe(III)(C_2O_4)_2^-$ is predicted by DFT and UHF to have a structure similar to $Fe(II)(C_2O_4)_2^{2-}$; however, the calculated Fe−O bond distances in $Fe(II)(C_2O_4)_2^{2-}$ are about 0.1 A shorter than those in $Fe(II)(C_2O_4)_2^{2-}$. DFT calculations predict that the Fe−O bond length of $Fe(III)(C_2O_4)_2^-$ is 1.90 Å for this tetrahedral-like transient complex. These Fe−O bond lengths are shorter than the Fe(III)−O 2.00 Å bond length of the parent and much shorter than the Fe(II)−O of 2.11 Å, but very close to our experimental values of 1.87−1.93 Å determined for the 4−115 ps transients after excitation. The reaction shown in 2a may reasonably explain the 4−115 ps time-resolved EXAFS data.

$$[Fe(C_2O_4)_3^{3-}]^* \rightarrow Fe(III)(C_2O_4)_2^- + 2CO_2\cdot^- \quad (2a)$$
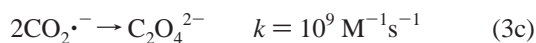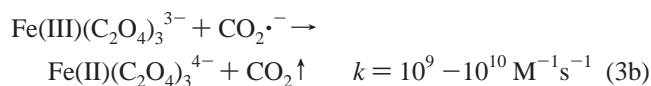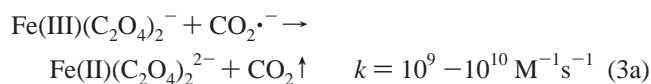
In addition, the Fe(III)−O bond length of the $(C_2O_3)O-Fe(III)(C_2O_4)_3^{3-}$ five-coordinate complex was calculated and found to have a value of 1.87 Å for a single Fe−ox bond and

2.00 Å for a two Fe—ox bond connection. To distinguish between reaction 2 and 2a is rather difficult because the dissociation process is very fast, less than 3 ps. From our EXAFS data, we determine a Fe—O bond distance, at +4 ps, of 1.93 Å, which may be considered as due to either a 5-coordinated transient or a mixture of the excited-state and the 4-coordinated transient. The 1.93 Å and 1.87 Å bond lengths are assigned to the five- and four-coordinated Fe(III) complexes because the bond length usually decreases as the number of ligands decreases. This decrease in bond length is commensurate with the time-resolved EXAFS spectra, which reveal that the 1.93 Å Fe(III)—O bond transient is formed earlier than the Fe(III)—O 1.87 Å bond transient. Essentially, we propose that one bond is cleaved first, leaving the Fe(III)—O 1.93 Å five-coordinate transient; then the second bond is cleaved, resulting in the formation of the Fe(III)—O 1.87 Å transient shown in reaction 2. Therefore, we assigned the +9 ps Fe—O 1.87 Å transient to Fe(III)(C$_2$O$_4$)$_2^-$ four-coordinated transient species. The decay lifetime of Fe(III)(C$_2$O$_4$)$_2^-$ is longer than 115 ps; this is also consistent with the appearance of a new 420–500 nm intermediate formed during the first 610 ps and observed by optical transient absorption spectroscopy.

The difference in the Fe—O bond length determined by the theoretical calculations for Fe(III)(ox) and Fe(II)(ox) complexes listed in Table 1 is also consistent with our time-resolved EXAFS results. All examples that we found in the literature show that for Fe—O containing molecules the experimental value of the Fe(II)—O bond length is always longer than the corresponding Fe(III)—O bond length.[7,45] The shorter Fe—O bond distances observed for the intermediates suggest strongly that they belong to Fe(III)—O intermediates and not to species formed after electron transfer because electron transfer would yield an Fe(II) intermediate. This suggestion is based on the fact that the Fe—O bond length of Fe(II)—ox is longer than that of parent Fe(III)—ox and of all transient species that we detected and measured by ultrafast EXAFS.

We conclude, therefore, that the ultrafast EXAFS and optical results obtained support the mechanism that photoexcitation induces the cleavage of an oxalate ligand before electron transfer and the photoreaction does not involves Fe(II)—O formation in first 115 ps. The major structural changes several ps after excitation have been shown in Figure 7b.

(d) Ten ns to 1 μs after dissociation (reactions 3a–c).

$$\text{Fe(III)(C}_2\text{O}_4)_2^- + \text{CO}_2^{\bullet -} \rightarrow$$
$$\text{Fe(II)(C}_2\text{O}_4)_2^{2-} + \text{CO}_2\uparrow \quad k = 10^9 - 10^{10}\ \text{M}^{-1}\text{s}^{-1} \quad (3a)$$

$$\text{Fe(III)(C}_2\text{O}_4)_3^{3-} + \text{CO}_2^{\bullet -} \rightarrow$$
$$\text{Fe(II)(C}_2\text{O}_4)_3^{4-} + \text{CO}_2\uparrow \quad k = 10^9 - 10^{10}\ \text{M}^{-1}\text{s}^{-1} \quad (3b)$$

$$2\text{CO}_2^{\bullet -} \rightarrow \text{C}_2\text{O}_4^{2-} \quad k = 10^9\ \text{M}^{-1}\text{s}^{-1} \quad (3c)$$

After the dissociation of one oxalate, a CO$_2^{\bullet -}$ ion radical is formed, which absorbs below 350 nm[46] and therefore does not affect the visible transient absorption spectrum that we detected. The highly reactive CO$_2^{\bullet -}$ radical is known for its high redox potential ($E^0 = \sim -1.9$ V(NHE)),[47] which can react with Fe(III)(C$_2$O$_4$)$_2^-$, Fe(III)(C$_{24}$O$_4$)$_3^{3-}$, or recombine with another CO$_2^{\bullet -}$ radical according to reactions 3a–c.[48,49]

In this scheme, the reduction of Fe(III) to Fe(II) occurs after dissociation as a consequence of the diffusion-controlled intermolecular electron transfer from CO$_2^{\bullet -}$ to the Fe(III)(ox) complex. The decay lifetime of the 360–550 nm transient band

is also found to be diffusion-controlled and depend on concentrations; therefore, the electron-transfer process is intermolecular. The time required for electron transfer is $\sim 10^{-15}$ s once the optimized configuration for electron transfer is reached.[50] However, the observed intermolecular electron-transfer reaction rate was found to be close to the diffusion-controlled reaction rate. The decay rate was estimated to be in the 10^8–10^9 s^{-1} range, which is consistent with the observed 110 ns decay lifetime of the 360–550 nm band at 2.3 mM.
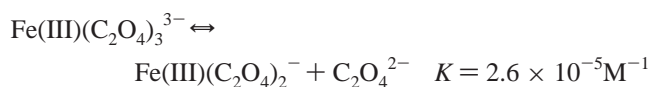
The observed spectra changes are assigned to reaction 3a, [Fe(III)(C$_2$O$_4$)$_2^-$ (λ_{max} = 430 nm) to Fe(II)(C$_2$O$_4$)$_2^{2-}$ (λ_{max} = 420–430 nm)] and reaction 3b, the formation of Fe(II)(C$_2$O$_4$)$_3^{4-}$ (λ_{max} = 400 nm). We also determined that the maximum absorption, λ_{max}, shifts to longer wavelengths with a decrease in the coordination number. Fe(II)(C$_2$O$_4$)$_2^{2-}$ has the same coordination number and similar λ_{max} as Fe(III)(C$_2$O$_4$)$_2^-$; however, when one additional oxalate is coordinated with the Fe(II), the λ_{max} of Fe(II)(C$_2$O$_4$)$_3^{4-}$ becomes shorter than the Fe(II)(C$_2$O$_4$)$_2^{2-}$ band maximum wavelength. The same phenomena are also found in fs optical transient spectra where a continuous shift of the absorption maximum from 400 to 430 nm occurs because of the formation of excited states and fast dissociation.

(e) μs to 2ms after dissociation (reaction 4):

$$\text{Fe(II)(C}_2\text{O}_4)_3^{4-} \leftrightarrow \text{Fe(II)(C}_2\text{O}_4)_2^{2-} + \text{C}_2\text{O}_4^{2-} \quad (4)$$

The long-lived component found in the ns to ms experiments has been suggested to be an Fe(II)(C$_2$O$_4$)$_3^{4-}$ transient,[5] which has a decay lifetime of 0.63 ms at 2.3 mM and 0.83 ms at 9.2 mM, in agreement with the literature values.[5,6] The equilibrium, eq 4, will obviously shift to the left when the concentration of oxalate increases and will result in a slower decay of Fe(II)(C$_2$O$_4$)$_3^{4-}$.[5,6]

3.3. Carbon Dioxide Anion Radical Scavenging. In both mechanisms I and II discussed in the introduction, C$_2$O$_4^{\bullet -}$/CO$_2^{\bullet -}$ radicals can react with Fe(III)(C$_2$O$_4$)$_3^{3-}$ parent molecules to form Fe(II)(C$_2$O$_4$)$_3^{4-}$. This is believed to be the reason for the well-known larger than one quantum yield for the formation of the Fe(II) product.[5] In mechanism I, the Fe(II) product can be produced by two different pathways: (a) directly by intramolecular electron transfer form the oxalate ligand to Fe(III) complex and (b) by intermolecular electron transfer from C$_2$O$_4^{\bullet -}$/CO$_2^{\bullet -}$ to ferrioxalate. However, in mechanism II, because the generation of Fe(II) could only occur by intermolecular electron transfer from CO$_2^{\bullet -}$ to Fe(III) complexes, the formation of the CO$_2^{\bullet -}$ radical shown in reaction 2 is the critical dominant component of the intermolecular electron-transfer reaction. Although equilibrium reactions between trioxalate and dioxalate complexes are known to occur in the steady-state ferrioxalate solution[51]

$$\text{Fe(III)(C}_2\text{O}_4)_3^{3-} \leftrightarrow$$
$$\text{Fe(III)(C}_2\text{O}_4)_2^- + \text{C}_2\text{O}_4^{2-} \quad K = 2.6 \times 10^{-5}\text{M}^{-1}$$

the electron-transfer process does not take place because no CO$_2^{\bullet -}$ radicals are produced in the dark at room temperature.

To distinguish between mechanisms I and II, Cooper et al.[5] suggested CO$_2^{\bullet -}$ radical-scavenging experiments. Considering both mechanisms, it is evident that the quenching of CO$_2^{\bullet -}$ by radical scavengers, other than ferrioxalate, will result in the reduction of the Fe(II) yield. Because the intramolecular electron-transfer process is not affected by radical-scavenging reactions, the decrease in the Fe(II) amount formed will not

EXAFS Transient Structures and Kinetics of Fe(III)ox

J. Phys. Chem. A, Vol. 111, No. 38, 2007 **9333**

exceed 50% if mechanism I is the only mechanism. If mechanism II is dominant, then a significant decrease, more than 50%, in the quantum yield of the Fe(II) formed is expected to be observed when most carbon dioxide ion radicals have been scavenged. The first attempt to scavenge $CO_2 \cdot^-$ was made by Cooper et al. using isopropanol as the radical scavenger. However, only a 10% reduction in the quantum yield of Fe(II) was observed.[5] Further improvement was achieved by using glycol,[52] which could act because of its high viscosity as both a radical scavenger and a molecular-reorientation retarder. The quantum yield of Fe(II) was found to decrease from 1.0 to around 0.1 with increasing concentration of glycol in the ferrioxalate solution irradiated at 436 nm. The photolysis reaction of ferrioxalate in dimethylformate, a solvent that is reported to form cation radicals when irradiated with 365−436 nm light,[53] was found to decrease the quantum yield of Fe(II) formed to 0.69,[54] compared to 1.16−1.26[8] observed in pure H_2O solution irradiated at the same wavelength.

The carbon dioxide anion radical was found to induce one-electron reduction of thymine and its derivatives, in water solution, by nucleophilic addition.[55] Therefore, we used thymine as an effective $CO_2 \cdot^-$ radical scavenger. The amount of Fe(II) product formed, which is proportional to the optical density of the $[Fe(II)(phen)_3]^{2+}$ complex that absorbs with λ_{max} at 510 nm. Ferrioxalate mixed with several concentrations of thymine as a function of irradiation time is shown in Figure 5. The square points represent the pure ferrioxalate solution (5.8×10^{-5} M) without thymine; the circle and triangle points represent ferrioxalate solution mixed with 1.25×10^{-5} M and 5.0×10^{-5} M thymine, respectively. After increasing the amount of thymine, the reaction of $CO_2 \cdot^-$ with thymine is expected to become competitive with the reaction of $CO_2 \cdot^-$ with ferrioxalate, and, as a result, the formation of the Fe(II) product is expected to decrease. The decrease in the amount of Fe(II) formed was found to depend on the concentration of thymine and the radical-scavenging effect starts to be observed when a small amount of thymine has been added to the ferrioxalate solution. When the ratio of the concentrations of thymine to ferrioxalate is about 1:4.5, a 48% decrease in the amount of Fe(II) formed was observed, compared to the value without thymine, when the solution was irradiated for 400 s, see Figure 5 (circle curve). Furthermore, when this ratio increased to about 1:1, shown by the triangle points in Figure 5, the reaction of $CO_2 \cdot^-$ with ferrioxalate became minor and the quantum yield of Fe(II) was reduced by 73%. Increasing the concentration of thymine further shows only small addition changes in the yield compared to that with 5.0×10^{-5} M thymine. The concentration dependence observed suggests that the reactions of $CO_2 \cdot^-$ with the Fe(III) complex are diffusion-controlled, which is a direct result of intermolecular electron transfer. Scavenging all of the $CO_2 \cdot^-$ radicals is difficult to achieve in this experiment because the reactions of $CO_2 \cdot^-$ with Fe(III) complexes are very fast, 10^9-10^{10} M^{-1} s^{-1}.[49] The large, more than 50%, decrease of the Fe(II) quantum yield by the addition of thymine as a $CO_2 \cdot^-$ radical scavenger strongly suggests that mechanism II is the primary photoredox reaction, which also supports the mechanism, proposed by us, of dissociation preceding electron transfer.

3.4. Electron Transfer. The time-resolved EXAFS and optical data also supported by the radical scavenging experimental data presented here have encouraged us to reexamine the effect that electron transfer between ligand and metal has on the structure of ferrioxalate molecules and reconsider the sequence of one electron transfer and ligand dissociation processes. After reviewing the data presented, we believe that
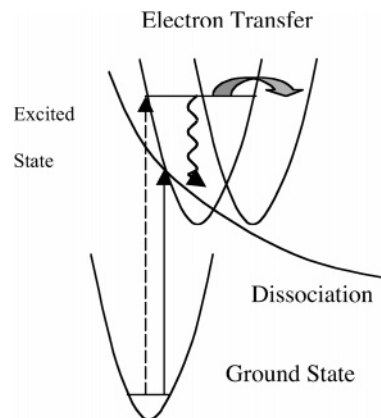
Figure 9. Potential energy diagram of initial electronic transitions within the charge-transfer band.

the primary reaction after excitation is ligand dissociation (mechanism II), which indicates that the dissociation reaction rate is much faster than the intramolecular electron-transfer rate. If the dissociation process that we propose is the dominant mechnism, then an interesting question arises: why does the redox reaction favor dissociation over electron transfer. This maybe due to the following:

(1) Excitation energy: The excitation energy (400 nm = 3.1 eV) used in our fs experiments is sufficient to break both Fe−O bonds and the C−C bond of the oxalate molecule. The absorption spectrum of ferrioxalate solution, Figure 6, exhibits a shoulder around 270 nm in what is called the charge-transfer (CT) band, which suggests that this CT band is composed of not only the transition between ground state and first excited-state but also includes several other upper excited states. A possible reason for the mechanism that we proposed rather than intramolecular electron transfer is that the 400 nm transition ($\epsilon = 160$ $cm^{-1}M^{-1}$) promotes the HOMO electron to a low-energy excited level of the CT band that crosses the dissociative potential surface, see Figure 9. To examine this hypothesis, we are performing the same optical and EXAFS experiments using the third, 267 nm, harmonic of Ti:Sapphire laser that excites the Fe(III)ox molecule closer to the 210 nm maximum absorption wavelength of the CT band. At such a higher excitation state, it may be possible that electron transfer or spin crossover might be more-dominant than dissociation. The ^{13}C isotope effect has been observed in the 366−520 nm range and is found to depend remarkably on the excitation energy.[10] This isotope is not found in the shorter than 366 nm region. This variation also suggested different photolysis pathways of the ferrioxalate at different excitation energies. It is possible that at higher excitation energies, the transition shown in Figure 9, by the dotted line may result in a slower predissociation than intramolecular electron-transfer rate (shown as curved down arrow). The higher excited state may promote the electron to a region of large overlap of the Fe(III)/Fe(II) electronic state potentials that facilitates fast electron transfer, see Figure 9. In this process, it is expected that the intramolecular electron-transfer rate will be high and therefore will be the primary process after excitation.

(2) Steric effect: Although the structure of $Fe(II)(C_2O_4)_3^{3-}$ is not known, a possible reason for the low electron-transfer efficiency is that the original Fe(III) and $C_2O_4^{2-}$ groups are not oriented properly for intramolcular electron transfer. To transfer an electron from the oxalate to the Fe(III), in-plane or out-of-plane nuclear movement may be necessary until the correct configuration is achieved that promotes electron transfer. The rate of intramolecular electron transfer also depends upon the

relative orientation of the iron and the oxalate groups. If the ferrioxalate molecule is rigid, then in the low-excitation-energy range (400 nm) the dissociation rate may be larger than the rate needed for the molecule to reorganize and achieve the correct configuration for electron transfer to take place.[50] Consequently, dissociation rather than intramolecular electron transfer will be the dominant reaction immediately after excitation. This type of orientation is in agreement with electron-transfer theories[56] in that the correct alignment between the electron donor and acceptor is required for efficient electron transfer to take place. Even though these theories address mostly intermolecular electron transfer, they should also apply to intramolecular electron-transfer processes. Because the six-coordinated $Fe(III)(ox)_3^{3-}$ ion is, geometrically, more rigid than the lower coordination $Fe(III)(ox)_n^{3-2n}(n < 3)$ complexes, its nuclear motion is expected to be restricted. Consequently, the expected higher steric barrier in the ferrioxalate may increase the electron-transfer activation energy and therefore may hinder the electron-transfer reaction and force it to proceed at a slower rate.

(3) Our data show that the Fe−O bond distance of the excited state for the covalent bond between iron and oxygen is elongated by about 10% after excitation, from 2.00 to 2.16 Å, which makes the bond weaker and therefore easier to break. Elongation by 0.2 Å of the excited-state bond was also observed for Fe(II)−N.[31] However, shortening by 0.06 Å was calculated by DFT for the excited state of Fe(III)−Cl.[57]

In summary, the most-compelling reason for proposing that dissociation precedes electron transfer is our observation that the Fe−O bond length of the initially formed transients measured by EXAFS are 1.93 and 1.87 Å, which correspond to Fe(III)−O rather than Fe(II)−O. Other reasons for believing that the intramolecular electron transfer not being the primary reaction process after excitation at 400 nm are (1) the excitation energy is sufficient for dissociation; (2) the steric barrier for intramolecular electron transfer is high; (3) weakening of the Fe−O bond due to bond elongation; (4) strong $CO_2^{\bullet-}$ radical scavenging effect on the Fe(II) product yield; (5) UHF and DFT calculations support the EXAFS data. We expect that exciting the $Fe(III)(ox)_3^{3-}$ complex at higher energy, 267 nm, where the Fe(III)/Fe(II) states overlap is larger, the reason for the observed order of the electron transfer and dissociation processes might became more understood.

4. Conclusions

We propose, based on ultrafast optical data, EXAFS data, radical-scavenging results, and theoretical calculations that the ferrioxalate photo redox reaction involves predominantly a fast dissociation process instead of intramolecular electron transfer. We believe that these data provide the first experimental and theoretical evidence for electron transfer not being the primary, initial process, but rather follow dissociation.

References and Notes

(1) Draper, J. *Philos. Mag.* **1857**, *51*, 161.

(2) Allmand, A. J.; Webb, W. W. *J. Chem. Soc.* **1929**, 1518.

(3) Livingston, R. *J. Phys. Chem.* **1940**, *44*, 601.

(4) Parker, C. A.; Hatchard, C. G. *J. Phys. Chem.* **1959**, *63*, 22.

(5) Cooper, G. D.; DeGraff, B. A. *J. Phys. Chem.* **1971**, *75*, 2897.

(6) Nadtochenko, V.; Kiwi, J. *J. Photochem. Photobiol., A* **1996**, *99*, 145.

(7) Chen, J.; Zhang, H.; Tomov, I. V.; Ding, X. L.; Rentzepis, P. M. *Chem. Phys. Lett.* **2007**, *437*, 50.

(8) Hatchard, C. G.; Parker, C. A. *Proc. R. Soc. London, Ser. A* **1956**, *235*, 518.

(9) Patterso, Ji; Perone, S. P. *J. Phys. Chem.* **1973**, *77*, 2437.

(10) Betts, R. H.; Buchannon, W. D. *Can. J. Chem.* **1976**, *54*, 2577.

(11) Parker, C. A. *Trans. Faraday Soc.* **1954**, *50*, 1213.

(12) Jamieson, R. A.; Perone, S. P. *J. Phys. Chem.* **1972**, *76*, 830.

(13) Ingram, D. J. E.; Hodgson, W. G.; Parker, C. A.; Rees, W. T. *Nature* **1955**, *176*, 1227.

(14) Oster, G.; Yang, N. L. *Chem. Rev.* **1968**, *68*, 125.

(15) Mulazzani, Q. G.; Dangelantonio, M.; Venturi, M.; Hoffman, M. Z.; Rodgers, M. A. J. *J. Phys. Chem.* **1986**, *90*, 5347.

(16) Rousse, A.; Rischel, C.; Gauthier, J. C. *Rev. Mod. Phys.* **2001**, *73*, 17.

(17) Tomov, I. V.; Chen, J.; Ding, X.; Rentzepis, P. M. *Chem. Phys. Lett.* **2004**, *389*, 363.

(18) Pfeifer, T.; Spielmann, S.; Gerber, G. *Rep. Prog. Phys.* **2006**, *69*, 443.

(19) Feurer, T.; Morak, A.; Uschmann, I.; Ziener, C.; Schwoerer, H.; Forster, E.; Sauerbrey, R. *Appl. Phys. B* **2001**, *72*, 15.

(20) Chen, J.; Tomov, I. V.; Elsayed-Ali, H. E.; Rentzepis, P. M. *Chem. Phys. Lett.* **2006**, *419*, 374.

(21) Rentzepis, P. M. *Chem. Phys. Lett.* **1968**, *2*, 117.

(22) *Time Resolved Diffraction*; Helliwell, J. R.; Rentzepis, P. M., Eds.; Oxford University Press: Oxford, 1997.

(23) Agarval, K. *X-Ray Spectroscopy*; Springer: New York, 1991.

(24) Raksi, F.; Wilson, K. R.; Jiang, Z. M.; Ikhlef, A.; Cote, C. Y.; Kieffer, J. C. *J. Chem. Phys.* **1996**, *104*, 6066.

(25) Chen, L. X.; Jager, W. J. H.; Jennings, G.; Gosztola, D. J.; Munkholm, A.; Hessler, J. P. *Science* **2001**, *292*, 262.

(26) Bressler, C.; Chergui, M. *Chem. Rev.* **2004**, *104*, 1781.

(27) Chen, L. X. *Annu. Rev. Phys. Chem.* **2005**, *56*, 221.

(28) Saes, M.; Bressler, C.; Abela, R.; Grolimund, D.; Johnson, S. L.; Heimann, P. A.; Chergui, M. *Phys. Rev. Lett.* **2003**, *90*, 047403.

(29) Campbell, L.; Mukamel, S. *J. Chem. Phys.* **2004**, *121*, 12323.

(30) Gawelda, W.; Johnson, M.; Groot, F. M. F. D.; Abela, R.; Bressler, C.; Chergui, M. *J. Am. Chem. Soc.* **2006**, *128*, 5001.

(31) Khalil, M.; Marcus, M. A.; Smeigh, A. L.; McCusker, J. K.; Chong, H. H. W.; Schoenlein, R. W. *J. Phys. Chem. A* **2006**, *110*, 38.

(32) Lee, T.; Jiang, Y.; Rose-Petruck, C. G.; Benesch, F. *J. Chem. Phys.* **2005**, *122*, 084506.

(33) Chen, L. X.; Shaw, G. B.; Novozhilova, I.; Liu, T.; Jennings, G.; Attenkofer, K.; Meyer, G. J.; Coppens, P. *J. Am. Chem. Soc.* **2003**, *125*, 7022.

(34) Chen, L. X.; Shaw, G. B.; Liu, T.; Jennings, G.; Attenkofer, K. *Chem. Phys.* **2004**, *299*, 215.

(35) Zhang, H.; Dvornikov, A. S.; Rentzepis, P. M. *J. Phys. Chem. A* **2005**, *109*, 5984.

(36) Oulianov, D. A.; Tomov, I. V.; Lin, S. H.; Rentzepis, P. M. *J. Chin. Chem. Soc.* **2001**, *48*, 127.

(37) Ravel, B.; Newville, M. *J. Synchrotron Radiat.* **2005**, *12*, 537.

(38) Merrachi, E. H.; Mentzen, B. F.; Chassagneus, F.; Bouix, J. *Rev. Chim. Miner.* **1987**, *24*, 56.

(39) Ankudinov, A. L.; Bouldin, C. E.; Rehr, J. J.; Sims, J.; Hung, H. *Phys. Rev. B* **2002**, *65*.

(40) Frisch, M. J.; Trucks, G. W.; Schlegel, H. B.; Scuseria, G. E.; Robb, M. A.; Cheeseman, J. R.; Montgomery, J. A., Jr.; Vreven, T.; Kudin, K. N.; Burant, J. C.; Millam, J. M.; Iyengar, S. S.; Tomasi, J.; Barone, V.; Mennucci, B.; Cossi, M.; Scalmani, G.; Rega, N.; Petersson, G. A.; Nakatsuji, H.; Hada, M.; Ehara, M.; Toyota, K.; Fukuda, R.; Hasegawa, J.; Ishida, M.; Nakajima, T.; Honda, Y.; Kitao, O.; Nakai, H.; Klene, M.; Li, X.; Knox, J. E.; Hratchian, H. P.; Cross, J. B.; Bakken, V.; Adamo, C.; Jaramillo, J.; Gomperts, R.; Stratmann, R. E.; Yazyev, O.; Austin, A. J.; Cammi, R.; Pomelli, C.; Ochterski, J. W.; Ayala, P. Y.; Morokuma, K.; Voth, G. A.; Salvador, P.; Dannenberg, J. J.; Zakrzewski, V. G.; Dapprich, S.; Daniels, A. D.; Strain, M. C.; Farkas, O.; Malick, D. K.; Rabuck, A. D.; Raghavachari, K.; Foresman, J. B.; Ortiz, J. V.; Cui, Q.; Baboul, A. G.; Clifford, S.; Cioslowski, J.; Stefanov, B. B.; Liu, G.; Liashenko, A.; Piskorz, P.; Komaromi, I.; Martin, R. L.; Fox, D. J.; Keith, T.; Al-Laham, M. A.; Peng, C. Y.; Nanayakkara, A.; Challacombe, M.; Gill, P. M. W.; Johnson, B.; Chen, W.; Wong, M. W.; Gonzalez, C.; Pople, J. A. *Gaussian 03*, revision C.02; Gaussian, Inc.: Wallingford, CT, 2004.

(41) Tamura, H.; Goto, K.; Yotsuyan, T.; Nagayama, M. *Talanta* **1974**, *21*, 314.

(42) Jeong, J. S.; Yoon, J. Y. *Water Res.* **2004**, *38*, 3531.

(43) Ohrstrom, L.; Michaud-Soret, I. *J. Phys. Chem. A* **1999**, *103*, 256.

(44) Deyrieux, R.; Peneloux, A. *Bull. Soc. Chim. Fr.* **1969**, *8*, 2675.

(45) *International Tables for Crystallography*, 3rd ed.; Prince, E., Ed.; Kluwer Academic: Dordrecht, 2004; Vol. C, p 786.

(46) Neta, P.; Simic, M.; Hayon, E. *J. Phys. Chem.* **1969**, *73*, 4207.

EXAFS Transient Structures and Kinetics of Fe(III)ox

J. Phys. Chem. A, Vol. 111, No. 38, 2007 **9335**

(47) Schwarz, H. A.; Dodson, R. W. *J. Phys. Chem.* **1989**, *93*, 409.
(48) Astruc, D. *New J. Chem.* **1992**, *16*, 305.
(49) Hislop, K. A.; Bolton, J. R. *Environ. Sci. Technol.* **1999**, *33*, 3119.
(50) Marcus, R. A. *Rev. Mod. Phys.* **1993**, *65*, 599.
(51) Jeong, J.; Yoon, J. *Water Res.* **2005**, *39*, 2893.
(52) Loginov, A. V.; Katenin, S. B.; Voyakin, I. V.; Shagisultanova, G. A. *Sov. J. Coord. Chem.* **1986**, *12*, 1621.

(53) Melnikov, M. Y.; Belevskii, V. N.; Belopushkin, S. I.; Melnikova, O. L. *Russ. Chem. Bull.* **1997**, *46*, 1245.
(54) Ionescu, S. G.; Oncescu, T. *J. Photochem.* **1983**, *23*, 45.
(55) Ito, T.; Hatta, H.; Nishimoto, S. *Int. J. Radiat. Biol.* **2000**, *76*, 683.
(56) Marcus, R. A.; Sutin, N. *Bioc. Biophys. Acta* **1985**, *811*, 265.
(57) Kennepohl, P.; Solomon, E. I. *Inorg. Chem.* **2003**, *42*, 696.